

## Article

# An Effective Spherical NF/FF Transformation Suitable for Characterising an Antenna under Test in Presence of an Infinite Perfectly Conducting Ground Plane

Flaminio Ferrara <sup>1</sup>, Claudio Gennarelli <sup>1</sup>, Rocco Guerriero <sup>1,\*</sup> and Giovanni Riccio <sup>2</sup>

<sup>1</sup> Department of Industrial Engineering, University of Salerno, Via Giovanni Paolo II, 84084 Fisciano, Italy; flferrara@unisa.it (F.F.); cgennarelli@unisa.it (C.G.)

<sup>2</sup> Department of Information and Electrical Engineering and Applied Mathematics, University of Salerno, Via Giovanni Paolo II, 84084 Fisciano, Italy; griccio@unisa.it

\* Correspondence: rguerriero@unisa.it; Tel.: +39-089-96-4259

**Abstract:** An effective near-field to far-field transformation using a reduced number of near-field measurements collected via a spherical scan over the upper hemisphere, due to the presence of a flat metallic ground, is devised in this paper. Such a transformation relies on the non-redundant sampling representations of electromagnetic fields and exploits the image principle to properly account for the metallic ground, supposed to be of infinite extent and realised by perfectly conducting material. The sampling representation of the probe voltage over the upper hemisphere is developed by modelling the antenna under test and its image by a very adaptable convex surface, which is able to fit as much as possible the geometry of any kind of antenna, thus minimising the volumetric redundancy and, accordingly, the number of required samples as well as the measurement time. Then, the use of a two-dimensional optimal sampling interpolation algorithm allows the reconstruction of the voltage value at each sampling point of the spherical grid required by the classical near-field-to-far-field transformation developed by Hansen. Numerical examples proving the effectiveness of the developed sampling representation and related near-field-to-far-field transformation techniques are reported.

**Keywords:** antenna characterisation; near-field-to-far-field transformation; spherical scanning; infinite metallic ground plane; image principle; non-redundant representations of electromagnetic fields; flexible antenna modelling



**Citation:** Ferrara, F.; Gennarelli, C.; Guerriero, R.; Riccio, G. An Effective Spherical NF/FF Transformation Suitable for Characterising an Antenna under Test in Presence of an Infinite Perfectly Conducting Ground Plane. *Electronics* **2024**, *13*, 397. <https://doi.org/10.3390/electronics13020397>

Academic Editor: Dimitra I. Kaklamani

Received: 20 December 2023

Revised: 10 January 2024

Accepted: 16 January 2024

Published: 18 January 2024



**Copyright:** © 2024 by the authors. Licensee MDPI, Basel, Switzerland. This article is an open access article distributed under the terms and conditions of the Creative Commons Attribution (CC BY) license (<https://creativecommons.org/licenses/by/4.0/>).

## 1. Introduction

The design and manufacturing processes of an antenna require, as a crucial step, its characterization. Indeed, it is a very challenging task since the characteristics of the antenna (frequency, electric dimension, far-field angular coverage, environmental conditions, etc.) and the intended application determine the choice of the measurement technique to be used that guarantees the greatest accuracy [1]. The pros and cons of far-field versus near-field test ranges are well known to the antenna measurement community. The far-field test ranges are usually employed when dealing with antennas working at low frequencies, and only the far-field (FF) pattern in the principal planes is required. Near-field (NF) test setups are instead used when dealing with antennas working at higher frequencies, and complete FF pattern evaluations and polarisation measurements are required. Note that, unlike NF test setups, the FF test range is usually an outdoor setup and has the disadvantage that the weather conditions and surroundings (buildings, hills, objects, electromagnetic interference from other wireless networks) can impair the accuracy of the measurements. Nevertheless, the use of the NF test setups requires a greater number of measurements than the FF ones, since the collected measurements have to be properly post-processed through a NF/FF transformation to obtain the FF pattern in any desired cut plane. The choice of the NF

test setup to be used is always a trade-off between the type of antenna, the measurement requests, and the involved analytical and mechanical complexities. Accordingly, the planar NF test setup is usually chosen to characterise high-directivity antennas under test (AUTs); the cylindrical NF test setup is well-suited for AUTs mainly radiating in an angular zone centred on the horizontal plane; the spherical NF test setup is particularly recommended for AUTs without preferential radiation directions. Obviously, depending on the NF test setup adopted to characterise the antenna under test (AUT), the NF/FF transformation employed to evaluate the FF pattern can be planar, cylindrical, or spherical [1–8]. It must be stressed that the spherical NF test setup shows the greatest mechanical complexity, and the related NF/FF transformation is analytically the most complex. In any case, it can be adopted to characterise any kind of antennas, allowing a FF characterization over the whole FF sphere without any truncation error, and, accordingly, can be considered the purest and most complete NF antenna measurement solution. This is the reason why, over the years, it has attracted the attention of the antenna measurements community (see [9–32] as a non-exhaustive list of references). In particular, many efforts have been devoted to developing NF/FF transformations with spherical scan using sampling techniques more efficient from a data reduction viewpoint than the classical NF/FF transformation developed by Hansen in [15]. As a matter of fact, this last makes use of a spherical sampling grid, in which the number of parallels and that of the samples along each parallel are related, according to “the minimum sphere rule,” to the radius of the minimum sphere containing the AUT. Obviously, the larger the AUT size, the greater the number of measurements and, as a consequence, the longer the acquisition time. The theoretical results concerning the non-redundant sampling representations of the radiated or scattered electromagnetic (EM) fields [33] have been exploited to develop NF/FF transformations [16,26–28], which make use of a smaller number of measurement points as compared to that utilised by classical Hansen’s technique [15]. These techniques have proven to be effective from a numerical and experimental standpoint without impairing the accuracy of the FF reconstruction process. This has been made possible since, according to [33], it is possible to adopt an effective non-redundant sampling representation of the voltage, which makes use of a minimum set of NF samples, whose number depends on the convex surface chosen to model the considered AUT. These voltage samples are then interpolated by an “ad hoc” two-dimensional optimal sampling interpolation (OSI) formula to reconstruct the voltage values that the measuring probe would have collected at the sampling points of the classical spherical grid, thus allowing one to get the FF pattern via Hansen’s NF/FF transformation technique. The choice of the modelling surface is crucial for obtaining a sampling representation that is really non-redundant and substantially depends on the given AUT, since the choice criterion is that the modelling surface is chosen such that it adheres as much as possible to its actual geometry. Thus, the modelling surface has been chosen in [16,26,27] coincident with that of an oblate spheroid [16,27] or that obtained by two circular bowls sharing the apertures and with eventually different lateral bendings (double bowl modelling) [26] to characterise a quasi-planar AUT, while in [16,26,27] a prolate spheroidal surface [16,27] or that bounding a cylinder terminated by two hemispherical caps (rounded cylinder) [26] has been adopted for a long AUT.

A very adaptable surface, bounding a central cylindrical body ended by two circular bowls with the same apertures and different bases, has been recently proposed [34] to characterise 3-D modular AUTs. As a matter of fact, it is able to best shape the geometry of such a kind of antenna, as well as any volumetric AUTs, by properly setting the height and the radius of the central body and the radii of the lateral bendings, thus minimising the volumetric redundancy, as well as the amount of the required measurements to be collected, as compared to a spherical modelling of the source. Note that such a surface has four degrees of freedom in the choice of the geometrical parameters and contains the surfaces bounding a rounded cylinder, a double bowl, and a sphere as particular cases.

The characterization of large and heavy AUTs in spherical NF setups requires the use of mechanically stable supports in order to ensure high repeatability of the measurements.

In such a case, the size and weight of the considered AUT do not allow one to satisfy such a requirement. This occurs when testing one or more antennas mounted on a large platform or integrated with the body of a car or aircraft, and the interest is not just to test the single antennas but the whole structure (antenna plus platform/vehicle) in order to assess its capability to build up the wireless link with the network infrastructure (terrestrial or satellite network) for which it is intended in its operating conditions. To meet such a goal, the considered radiating structure can be characterised through a hemispherical NF setup, wherein such a structure is placed on a turning metallic ground, providing the required well-defined measurement environment to ensure a high degree of repeatability, and the NF measurements are collected by the measuring probe, guided along a circular arc or mounted on a rotating gantry, over the upper hemisphere. Obviously, the NF data at the points of the spherical sampling grid required by Hansen's NF/FF transformation technique falling over the lower hemisphere must be set to zero, thus impairing the accuracy of FF reconstructions, which will be affected by a severe truncation error. This issue can be overcome, as proposed in [35,36], by applying the principle of image [37] in the presence of an infinitely perfectly electric conducting (PEC) ground plane for synthesising the lacking NF data over the lower hemisphere. Such a suggestion has been followed in [38,39] to develop non-redundant NF/FF transformations with a hemispherical scan for long AUTs.

The aim of this paper is to develop, according to the sampling strategy proposed in [38,39], a non-redundant NF/FF transformation with a hemispherical scan suitable for characterising volumetric AUTs whose encumbrance has one or two predominant dimensions as compared to the other one(s). Such a transformation technique makes use of the principle of image [37] to account for the PEC ground plane, which is supposed to be of infinite extent, and employs the adaptable surface developed in [34] to model the AUT and its image. It is possible to properly develop an efficient sampling representation over a sphere, wherein the sampling points lying on the upper hemisphere are the measurement points and the points belonging to the lower hemisphere are those at which the NF data have to be synthesised. A 2-D OSI algorithm, which allows the accurate reconstruction of the NF data needed by Hansen's NF/FF transformation technique, is also developed.

The paper is organised as follows: In Section 1, the interests and motivations for developing a non-redundant NF/FF transformation from NF data collected in the presence of a PEC ground plane and using very flexible antenna modelling to fit volumetric AUTs are stressed. In Section 2, an effective sampling representation of the voltage acquired by the probe over the scanning hemisphere is developed by properly applying the non-redundant representations of EM fields [33], by exploiting the principle of image [37] to account for the infinite PEC ground plane and by assuming the AUT and its image as contained in the adaptable surface developed in [34]. A two-dimensional OSI formula allowing one to accurately reconstruct the probe voltage at any point on the scanning sphere from a non-redundant number of its samples collected over the upper hemisphere is also developed in the same section. Numerical results assessing the accuracy of the developed OSI representation and of the corresponding NF/FF transformation are reported in Section 3. At last, Section 4 collects the conclusions.

## 2. Sampling Representation over the Upper Hemisphere

Let us characterise a large and heavy AUT through a spherical NF setup. The scanning is realised by combining the azimuthal movement of a metallic turntable, which can be conveniently modelled as a PEC plane with infinite extension, with the elevation motion of a small first-order measurement probe, guided along a circular arc or mounted on a rotating gantry. Accordingly, the considered probe, which possesses the same bandwidth as the AUT one [40], collects the NF measurements over the upper hemisphere of radius  $R_{hs}$  in presence of an infinite PEC ground plane (Figures 1 and 2). Let us introduce a spherical coordinate system  $(r, \theta, \varphi)$  having its origin  $O$  on the infinite PEC ground and coincident with the centre of the spherical measurement system to denote any observation point  $Q$ . Moreover, let us suppose that the considered AUT is  $d_{ag}$  away from the ground plane.

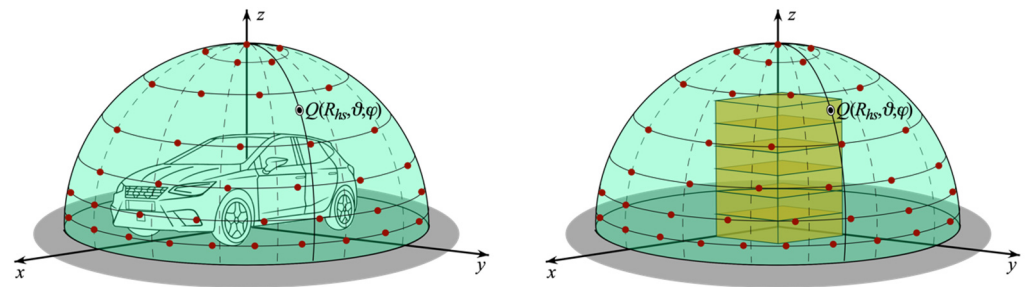


Figure 1. Spherical scan of heavy volumetric AUTs over a PEC ground plane.

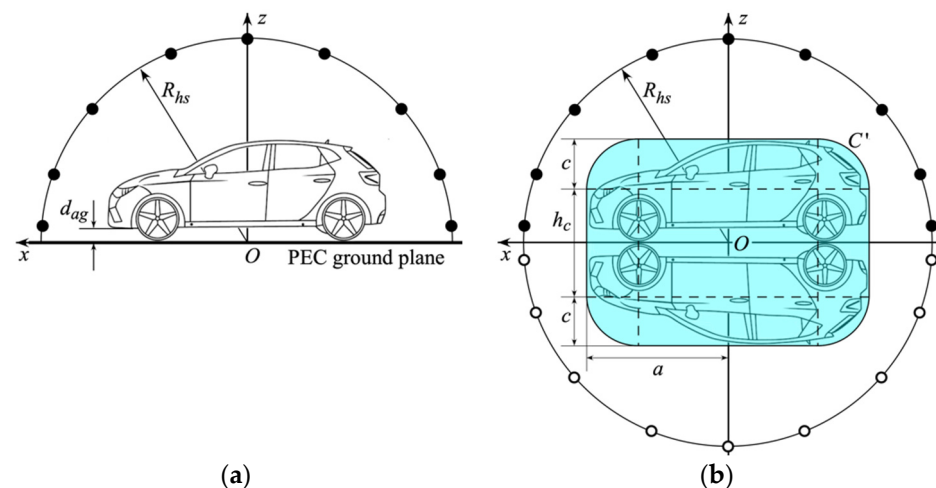


Figure 2. View in the meridian plane at  $\varphi = 0$ : (a) original formulation of the problem; (b) equivalent formulation of the problem.

The non-redundant sampling representation over the scanning hemisphere is developed by reformulating the problem according to the principle of image [37], which provides a convenient way to study a radiating structure in the presence of an infinite PEC ground plane. As a matter of fact, it enables us to consider, instead of the original problem (Figure 2a), an equivalent one (Figure 2b), wherein the infinite PEC ground plane is substituted by the image of the AUT above it. The AUT image is below the ground plane at the same distance as the AUT is above it, in order that the boundary condition of the equivalent problem is equal to the PEC boundary condition of the original problem. Accordingly, the AUT and its image can be considered together in the equivalent problem as a single combined AUT.

To fulfil the requirements of the non-redundant representations of EM fields [33], (i) the combined AUT (the considered AUT plus its image) has to be modelled by a convex surface,  $\Sigma_M$ , which fits as much as possible its actual geometry; (ii) each meridian and parallel describing the spherical observation surface must be represented in terms of a convenient parameter  $\tau$ ; and (iii) a suitable phase factor  $e^{j\gamma(\tau)}$  has to be determined in order to introduce the so-called “reduced voltage”

$$\tilde{V}(\tau) = \tilde{V}_{p,r}(\tau) = V_{p,r}(\tau)e^{j\gamma(\tau)} \tag{1}$$

with  $V_p, V_r$  denoting the voltage at the terminals of the probe in two of its orientations (in the second one, the probe is rotated by  $90^\circ$  around its axis). Such a reduced voltage is particularly convenient since, despite the mere voltage, it exhibits the features of a bandlimited function [33]. Indeed, it is only quasi-bandlimited, but it can be shown [33] that a very small error is made if  $\tilde{V}(\tau)$  is approximated by a rigorously bandlimited function. To this end, its bandwidth  $W_\tau$  is increased by a factor  $\chi'$ , named excess bandwidth factor,

which is able to control the aliasing error [33]. A  $\chi'$ -factor slightly greater than unity is enough when considering AUTs of large size, as those here considered.

The combined AUT of the equivalent problem can be considered a volumetric antenna, whose encumbrance has one or two predominant dimensions as compared to the other one(s), depending on the shape of the original antenna and its distance from the PEC ground. In order to choose the modelling surface  $\Sigma_M$  able to best fit the real geometry of the combined AUT, whatever its encumbrance, the very adaptable surface proposed in [34] can be conveniently employed. Due to the geometry of the equivalent problem, the here adopted one bounds a central cylindrical body of radius  $a$  and height  $h_c$ , which ends into two circular bowls with same aperture radii  $a$  and lateral bending radii  $c$  (see Figure 2b). These parameters can be properly set to minimise the volumetric redundancy, and accordingly, the number of required samples. Note that, by setting  $h_c = 0$  and  $c = a$ , the adaptable surface  $\Sigma_M$  reduces to the spherical one; by choosing  $h_c = 0$ ,  $\Sigma_M$  becomes the surface bounding a double bowl; and by setting  $c = a$ , the surface  $\Sigma_M$  reduces to that bounding a rounded cylinder.

Now, having properly modelled the combined AUT, each of the curves (meridian and parallel) of the observation surface has to be described according to the non-redundant representations framework [33] by choosing the bandwidth  $W_\tau$  and determining the optimal parameter  $\tau$  and phase function  $\gamma$ .

In the case of a meridian, the bandwidth is chosen to be equal to

$$W_\tau = \frac{\ell'}{\lambda} \tag{2}$$

where  $\ell'$  is the length of the curve  $C'$ , obtained by intersecting the meridian plane passing through  $Q$  with  $\Sigma_M$  and equal to  $2[h_c + (a - c) + \pi c]$ , and  $\lambda$  the wavelength. Then, the optimal parameter  $\tau$  and phase function  $\gamma$  are [33,34]:

$$\tau = (\pi/\ell') [\overline{QQ}_1 + \sigma'_1 - \overline{QQ}_2 + \sigma'_2] \tag{3}$$

$$\gamma = (\pi/\lambda) [\overline{QQ}_1 + \sigma'_1 + \overline{QQ}_2 - \sigma'_2] \tag{4}$$

where  $\overline{QQ}_1$  and  $\overline{QQ}_2$  are the distances from  $Q$  to tangency points  $Q_{1,2}$  on  $C'$  and  $\sigma'_{1,2}$  the corresponding curvilinear abscissae. Note that relations (3) and (4) depend on the position of  $Q$  when moving from 0 to  $\pi$ , since the distances  $\overline{QQ}_{1,2}$  and the corresponding curvilinear abscissae  $\sigma'_{1,2}$  change accordingly. Five cases occur in such a case, whose details can be found in [34].

In the case of a parallel, it can be easily shown [33,34] that  $\gamma$  is constant and that the optimal parameter  $\tau$  to be used to represent it is the azimuthal parameter  $\varphi$ . The corresponding bandwidth is:

$$W_\varphi = \frac{\pi}{\lambda} \max_{z'} D(M - D_m) = \frac{\pi}{\lambda} \max_{z'} \left( \sqrt{(z - z')^2 + (\rho + \rho'(z'))^2} - \sqrt{(z - z')^2 + (\rho - \rho'(z'))^2} \right) \tag{5}$$

where  $D_M, D_m$  are the maximum and minimum distances from the considered parallel to the circumference of  $\Sigma_M$  at  $z'$ ,  $\rho = R_{hs} \sin \vartheta$ , and  $\rho'(z')$  represents the equation of  $\Sigma_M$  in cylindrical coordinates. It can be easily proved [34] that the wanted maximum is in the zone of the surface  $\Sigma_M$  lying on the same side of the considered parallel with regard to its maximum transverse circumference. Such a maximum is reached at  $z' = z$  if  $|z| < h_c/2$ . If  $|z| > h_c/2$ , it is sought as the value of the angular coordinate  $\alpha$  such that

$$\begin{cases} z' = h_c/2 + c \cos \alpha; & \rho' = a - c + c \sin \alpha & \text{if } z > h_c/2 \\ z' = -(h_c/2 + c \cos \alpha); & \rho' = a - c + c \sin \alpha & \text{if } z < -h_c/2 \end{cases} \tag{6}$$

for which  $\partial(D_M - D_m)/\partial\alpha = 0$ .

The use of the above non-redundant parameters allows one to determine the arrangement of the sampling points over the whole observation sphere, since they have been

derived by considering the equivalent problem. Anyhow, only the NF sampling points belonging to the upper hemisphere can be reached in practice due to the presence of the infinite PEC ground plane. As will be shown later, the OSI algorithm also requires knowledge of those samples falling in the lower hemisphere; otherwise, they have to be set to zero, thus determining a severe truncation error in the reconstruction of the NF data required by Hansen’s NF/FF transformation. Again, the application of the image principle offers the possibility of overcoming this issue. As a matter of fact, these missing samples, which should have been acquired by the probe and rotated probe, can be synthesised from the corresponding ones collected on the upper hemisphere by applying the following “mirroring rule”:

$$\begin{cases} V_p(r, \pi - \vartheta, \varphi) = -V_p(r, \vartheta, \varphi) \\ V_r(r, \pi - \vartheta, \varphi) = V_r(r, \vartheta, \varphi) \end{cases} \tag{7}$$

which has been properly developed for the first-order probe adopted here.

It must be stressed that, to make possible the mirroring of the collected voltage samples according to (7), the sample arrangement must be symmetrically distributed with respect to the plane  $z = 0$  and must not contain the equator as sampling parallel due to the presence in that plane of the infinite PEC ground plane.

The NF samples directly acquired on the upper hemisphere and those mirrored via (7) are efficiently interpolated to obtain the NF data needed by Hansen’s NF/FF transformation. To this end, the following two-dimensional OSI algorithm [33,34] is conveniently employed. It exploits two properly matched OSI expansions, one allowing the interpolation along the meridians and the other along the parallels. Both expansions use few samples nearest to the given output point. To reconstruct the voltage at a point  $Q$  of Hansen’s spherical grid, the algorithm works as follows: It considers the meridian passing through  $Q(\vartheta, \varphi)$  and uses the following OSI expansion along the parallels [33]

$$V(\tau_k, \varphi) = \sum_{j=j_0-q+1}^{j_0+q} V(\tau_k, \varphi_{j,k}) \Omega_{N_j}(\varphi - \varphi_{j,k}, \bar{\varphi}) D_{N_j''}(\varphi - \varphi_{j,k}) \tag{8}$$

to reconstruct the  $2p$  intermediate samples at the intersection points  $(\vartheta(\tau), \varphi)$  of the meridian at  $\varphi$  with the involved sampling parallels.

In (8),  $V(\tau_k = k\Delta\tau, \varphi_{j,k} = j\Delta\varphi_k)$  are the involved  $2q$  non-redundant voltage samples directly measured or synthesised on each of  $2p$  parallels over the spherical observation surface with steps

$$\Delta\tau = \frac{\pi}{K''}; \Delta\varphi_k = \frac{2\pi}{2N_j'' + 1} \tag{9}$$

where  $K'' + 1$  is the number of the parallels (poles included), symmetrically distributed with respect to the plane  $z = 0$ , with  $K'' = \lfloor \chi K' \rfloor + 1$  and necessarily odd to avoid the equator as a sampling parallel,  $2N_j'' + 1$  is the number of the samples on each of them,

$$K' = \lfloor \chi' W_\tau \rfloor + 1; N_j'' = \lfloor \chi N_j' \rfloor + 1 \tag{10}$$

$$N_j' = \lfloor \chi^* W_\varphi(\tau_k) \rfloor + 1; \chi^* = 1 + (\chi' - 1)[\sin \vartheta(\tau_k)]^{-2/3} \tag{11}$$

and  $\lfloor \cdot \rfloor$  is the floor function. Moreover,  $j_0 = \lfloor \varphi / \Delta\varphi_k \rfloor$  is the index of the sample nearest to each point intersecting the meridian at  $\varphi$ ,  $\bar{\varphi} = q\Delta\varphi_k$ ,  $N_j = N_j'' - N_j'$ ,  $\chi$  an oversampling factor needed to control the truncation error [33], and

$$\begin{aligned} D_{N_j''}(\varphi) &= \frac{\sin[(2N_j''+1)\varphi/2]}{(2N_j''+1)\sin(\varphi/2)}; \\ \Omega_{N_j}(\varphi, \bar{\varphi}) &= \frac{T_{N_j}[2\cos^2(\varphi/2)/\cos^2(\bar{\varphi}/2)-1]}{T_{N_j}[2/\cos^2(\bar{\varphi}/2)-1]} \end{aligned} \tag{12}$$

$T_{N_j}(\cdot)$  being the Tschebyscheff polynomial of degree  $N_j$ . Note that, in using expansion (8), there is no need to extract the phase factor since it is constant along each involved parallel.

The  $2p$  intermediate samples are then interpolated via the following OSI expansion along the meridians [33,34]

$$V(\vartheta, \varphi) = e^{-j\gamma(\tau(\vartheta))} \sum_{k=k_0-p+1}^{k_0+p} \tilde{V}(\tau_k, \varphi) \Omega_K(\tau - \tau_k, \bar{\tau}) D_{K''}^e(\tau - \tau_k) \quad (13)$$

to finally get the value of the voltage  $V$  at  $Q$ . In (13),  $k_0 = \lfloor \tau/\Delta\tau \rfloor$  is the index of the sample closest to  $Q$ ,  $\bar{\tau} = p\Delta\tau$ ,  $K = K'' - K'$ , and the other symbols have the same or analogous meanings as in (8), save for

$$D_{K''}^e(\tau) = \frac{2K'' - 1}{2K''} D_{K''-1}(\tau) \quad (14)$$

which is the Dirichlet function tailored for an even number of samples, needed to account for the symmetric distribution of the parallels with respect to the plane  $z = 0$ .

### 3. Numerical Results

In this section, some representative results numerically assessing the feasibility of the proposed spherical NF/FF transformation for characterising volumetric AUTs in the presence of an infinitely perfectly conducting ground plane are presented. In order to show the capability of the proposed AUT modelling to reduce volumetric redundancy and, as a consequence, the number of required NF samples, two different kinds of antennas have been considered. The former (Case A) is a volumetric AUT whose geometry is characterised by two predominant dimensions as, f.i., a parallelepiped having its width ( $W$ ) and length ( $L$ ) greater than the height ( $H$ ), while the latter (Case B) is a volumetric AUT having a predominant dimension as, f.i., a parallelepiped for which  $H > W, L$ .

The AUT of Case A has been properly arranged to simulate an automotive body. To this end, a rectangular parallelepiped surmounted by a rectangle has been considered. The parallelepiped, whose geometric centre lies on the  $z$ -axis of the adopted  $(x, y, z)$  reference system, has width  $W_x = 14 \lambda$ , length  $L_y = 35 \lambda$ , and height  $H_z = 6 \lambda$  and is located at  $2 \lambda$  from the PEC ground plane. The rectangle is  $4.5 \lambda$  above the parallelepiped and is  $14 \lambda$  wide and  $25 \lambda$  long. A planar array of elementary Huygens sources, spaced by  $\lambda/2$  and polarized along the  $z$ -axis, is located on each of the faces of the parallelepiped at  $y = 17.5 \lambda$  and  $y = -17.5 \lambda$ . Moreover, the rectangle surmounting the parallelepiped is covered by another planar array of Huygens sources spaced by  $\lambda/2$  and polarized along the  $y$ -axis. An open-ended WR430 rectangular waveguide, operating at 2.45 GHz, scans a hemisphere of radius  $R_{hs} = 30 \lambda$ . To account for the presence of the infinite ground plane and properly develop the non-redundant representation over the entire sphere, the proposed technique exploits the principle of image, according to which the voltage at any sampling point is due to the contributions from the AUT and its image. To properly simulate the NF samples, the image of the AUT has been obtained by mirroring each electric and magnetic dipole, realising an elementary Huygens source of the AUT. Then, the obtained combined AUT has been modelled by an adaptable surface having parameters  $a = 18.85 \lambda$ ,  $h_c = 16 \lambda$ , and  $c = 4.5 \lambda$ . Moreover, rule (7) has been used to synthesise the NF samples, which should have been measured by the probe and rotated probe on the lower hemisphere. The non-redundant sampling representation has been obtained by adopting  $\chi' = \chi = 1.10$ .

To test the precision of the proposed sampling strategy and of OSI algorithms (8) and (13) from a qualitative standpoint, Figures 3 and 4 show the comparisons of the exact and reconstructed normalised amplitudes and phases of the voltages  $V_p$  and  $V_r$  on the meridians at  $\varphi = 0^\circ$  and  $\varphi = 90^\circ$ . As can be seen, the recovered patterns over the upper hemisphere are in very good agreement with the exact ones and do not suffer from any truncation errors. For the sake of completeness, the recoveries of the amplitudes of  $V_p$  and  $V_r$  relevant to the

meridian at  $\varphi = 60^\circ$  are also reported in Figure 5. The effectiveness of the OSI algorithm is confirmed by the normalised mean-square reconstruction errors. Such errors have been obtained by comparing the exact and recovered values of  $V_p$  and  $V_r$  on a dense grid of the scanning hemisphere and normalizing them to the maximum voltage value over it. As shown in Figure 6, these errors, computed for  $\chi' = 1.10, \chi = 1.05, 1.10, 1.15$ , and  $p, q$  ranging from 2 to 11, decrease as  $\chi, p$ , and  $q$  increase. This provides a tool for properly choosing the sampling/OSI parameters for a given reconstruction error. Note that a very low reconstruction error of about  $-60$  dB occurs for the adopted sampling/OSI parameters  $\chi' = \chi = 1.10$  and  $p = q = 8$ . Such an error can be considered negligible if compared with the measurement one. Moreover, to investigate the algorithm stability, the NF samples have been simulated as corrupted with random errors. In particular, a background noise (having an amplitude bound to  $\Delta\zeta$  and an arbitrary phase) and an uncertainty of  $\pm \Delta\zeta_r$  in amplitude and  $\pm \Delta\psi$  in phase have been added to each exact NF sample over the upper hemisphere. Figure 7 shows the reconstructions of amplitude and phase on the meridian at  $\varphi = 90^\circ$  obtained from these error-affected samples, which assess the algorithm's stability even in a real measurement environment.

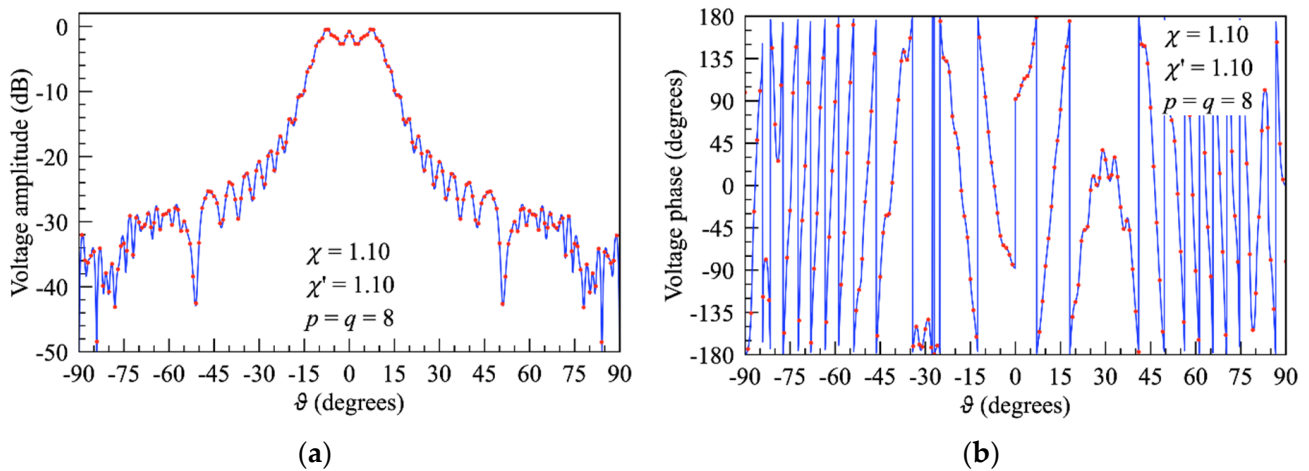


Figure 3.  $V_p$  on the meridian at  $\varphi = 0^\circ$ . Blue solid line: exact. Red dots: interpolated from the non-redundant samples: (a) Amplitude; (b) Phase.

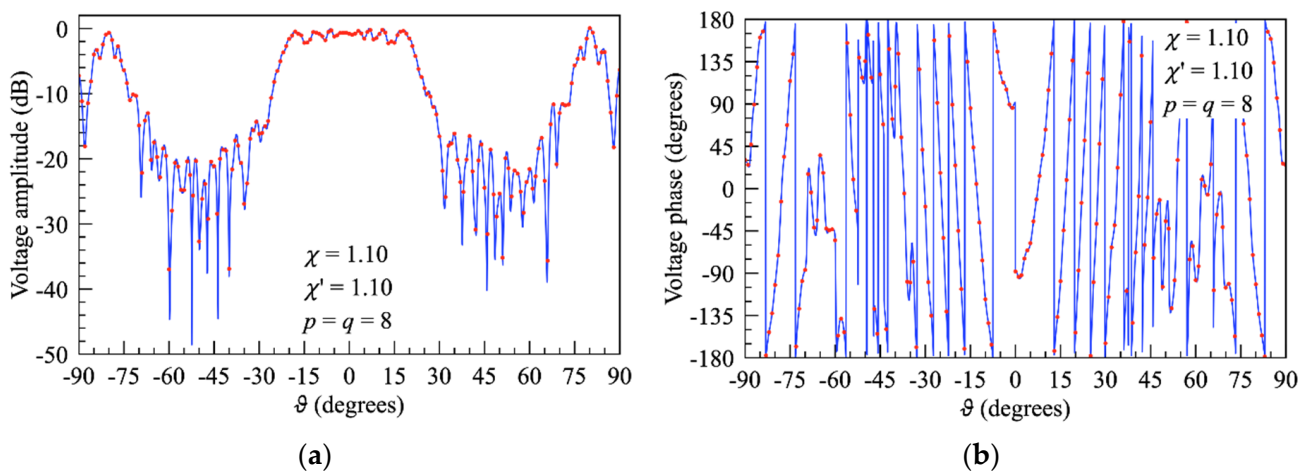


Figure 4.  $V_r$  on the meridian at  $\varphi = 90^\circ$ . Blue solid line: exact. Red dots: interpolated from the non-redundant samples: (a) Amplitude; (b) Phase.

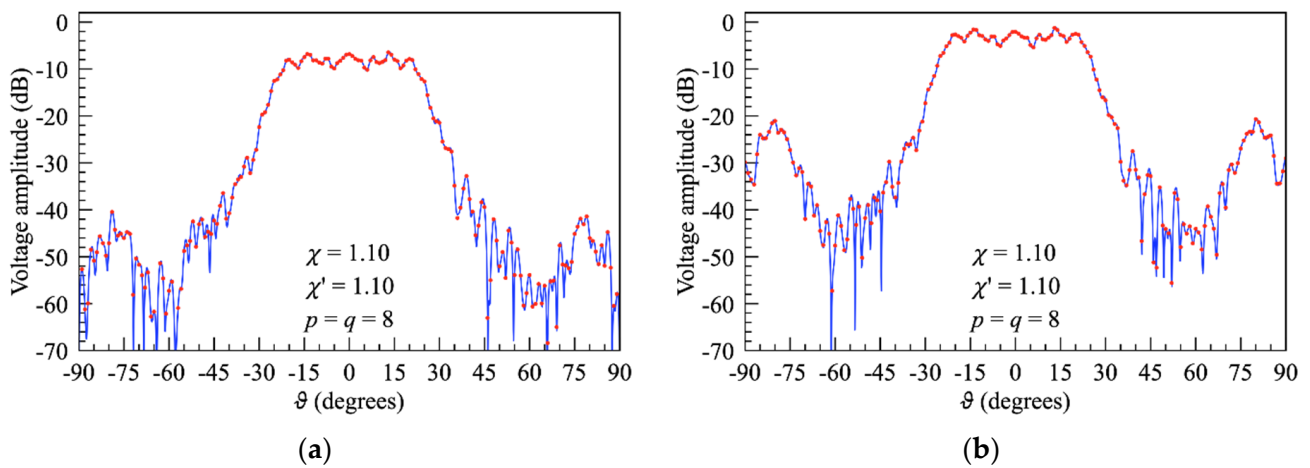


Figure 5. Voltage amplitude on the meridian at  $\varphi = 60^\circ$ . Blue solid line: exact. Red dots: interpolated from the non-redundant samples: (a)  $V_p$ ; (b)  $V_r$ .

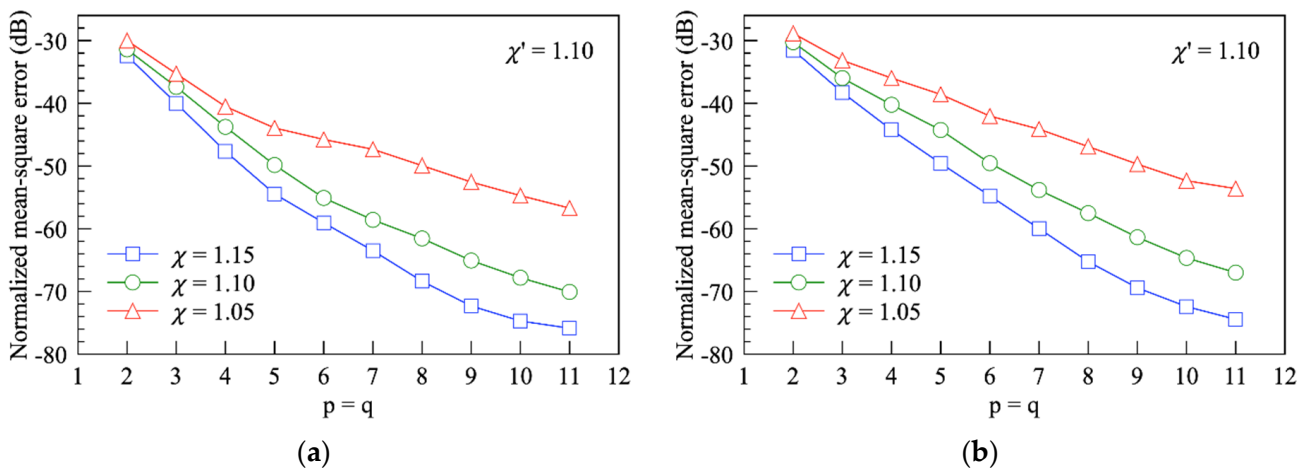


Figure 6. Normalised mean-square errors in the reconstruction of the probe voltage: (a)  $V_p$ ; (b)  $V_r$ .

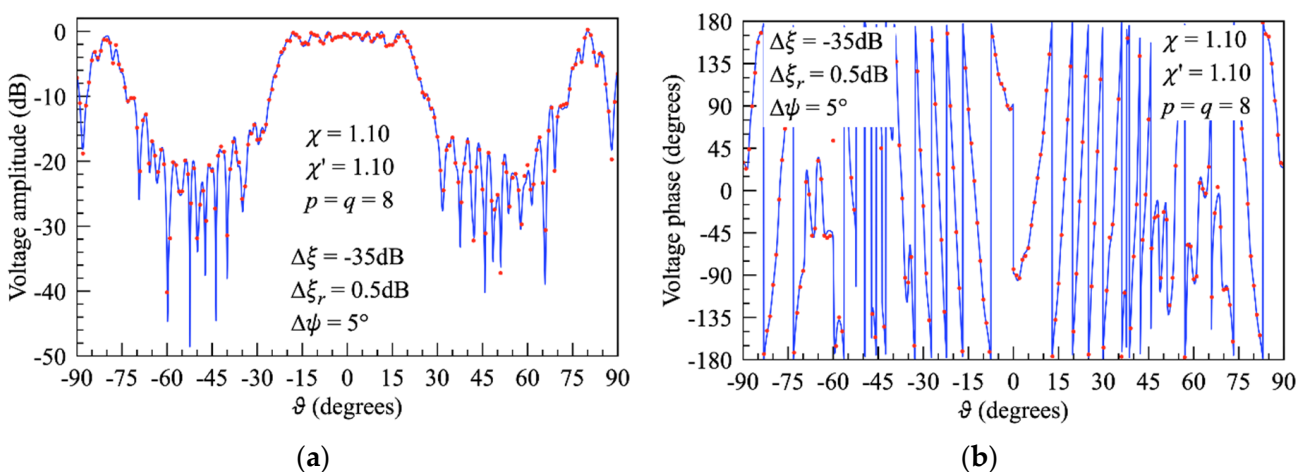
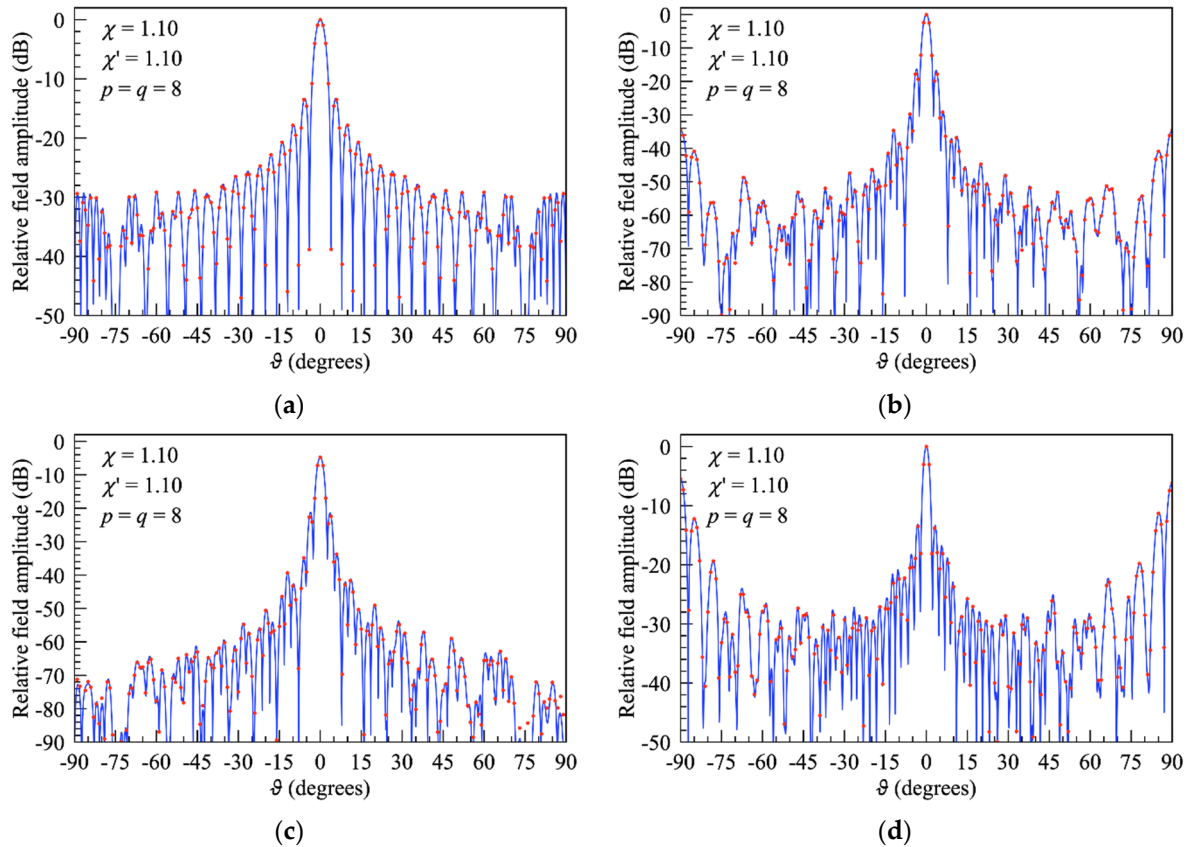


Figure 7.  $V_r$  on the meridian at  $\varphi = 90^\circ$ . Blue solid line: exact. Red dots: recovered from the error affected NF samples: (a) Amplitude; (b) Phase.

At last, OSI algorithms (8) and (13) have been adopted for recovering the NF data required to perform Hansen’s NF/FF transformation technique [15] from those collected and synthesised according to rule (7) at the points of the upper and lower hemispheres,

respectively, set by the developed sampling strategy. Figure 8 shows the comparisons between the recovered FF patterns in the cut planes at  $\varphi = 0^\circ$ ,  $60^\circ$ , and  $90^\circ$  and the corresponding exact ones over the upper hemisphere. As can be seen, the exact and recovered FF patterns agree very well, thus proving the efficiency of the devised NF/FF transformation with hemispherical scanning in the presence of an infinite PEC ground plane for volumetric AUT exhibiting two predominant dimensions.



**Figure 8.** Far-field pattern. Blue solid line: exact. Red dots: obtained from the non-redundant samples: (a)  $\varphi$ —component on the cut plane at  $\varphi = 0^\circ$ ; (b)  $\vartheta$ —component on the cut plane at  $\varphi = 60^\circ$ ; (c)  $\varphi$ —component on the cut plane at  $\varphi = 60^\circ$ ; (d)  $\vartheta$ —component on the cut plane at  $\varphi = 90^\circ$ .

The AUT of Case B has been properly arranged to simulate an antenna having a predominant dimension. To this end, a rectangular parallelepiped, with dimensions equal to  $(W_x \times L_y \times H_z) = (15\lambda \times 15\lambda \times 23\lambda)$  and having its centre on the  $z$ -axis of the used  $(x, y, z)$  reference system, has been considered. It is placed  $2\lambda$  away from the PEC ground plane, and its lateral faces are covered by planar arrays of elementary Huygens sources, spaced by  $\lambda/2$  and polarized along the  $z$ -axis. To simulate the combined AUT, the image of such an antenna with respect to the  $xy$  plane has been obtained as described in the previous example. Then, the combined AUT has been considered enclosed in the adaptable surface with parameters  $a = 10.6\lambda$ ,  $h_c = 50\lambda$ , and  $c = 2.5\lambda$ . The non-redundant sampling representation on the entire sphere has been obtained by adopting  $\chi' = \chi = 1.10$ . The NF samples at the corresponding sampling points have been simulated as acquired (or synthesised according rule (7)) on a sphere of radius  $R_{hs} = 35\lambda$ .

To qualitatively appreciate the effectiveness of OSI algorithms (8) and (13), the reconstruction of the voltage  $V_r$  on the meridian at  $\varphi = 90^\circ$  is shown in Figure 9. As can be seen, the reconstruction over the upper hemisphere is very accurate. The same accuracy is also experienced for the voltage reconstructions relevant to other meridians. These reconstructions are not shown here to save space. In any case, the accuracy of the devised strategy and of the related OSI algorithm can be appreciated by the normalised mean-square reconstruction

errors relevant to the voltage  $V_r$ , computed for  $\chi' = 1.10, \chi = 1.05, 1.10, 1.15, p$ , and  $q$  ranging from 2 to 11 and reported in Figure 10a. As can be seen, very low reconstruction errors (about  $-55$  dB) occur for the chosen sampling/OSI parameters. Moreover, the voltage reconstruction in Figure 10b relevant to the meridian at  $\varphi = 90^\circ$  and obtained from NF samples affected by random errors, as in a real measurement, assesses the robustness of the adopted OSI algorithm. The background noise and the uncertainty on each NF sample are the same as in the previous case.

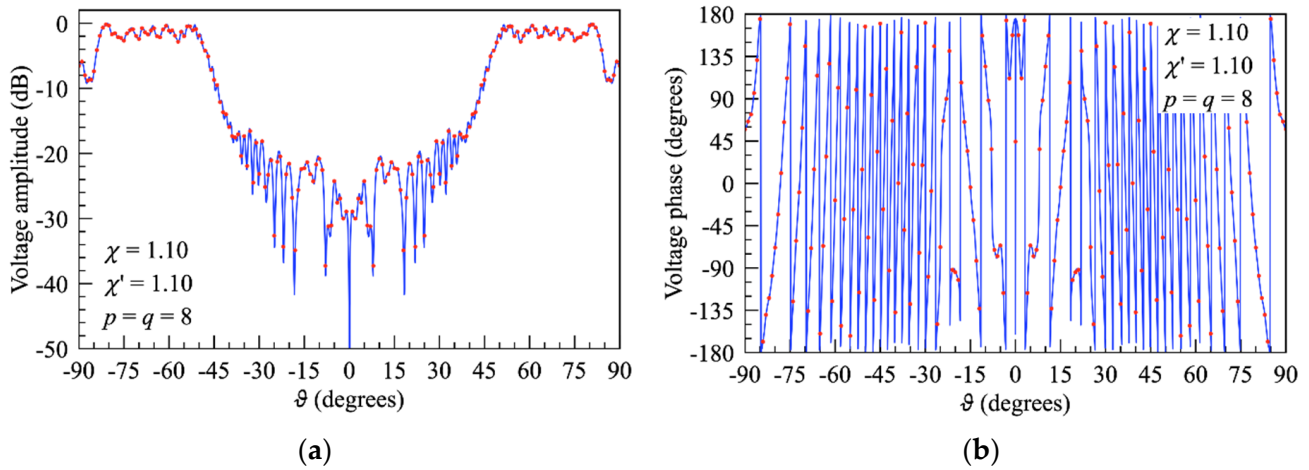


**Figure 9.**  $V_r$  on the meridian at  $\varphi = 90^\circ$ . Blue solid line: exact. Red dots: interpolated from the non-redundant samples: (a) Amplitude; (b) Phase.

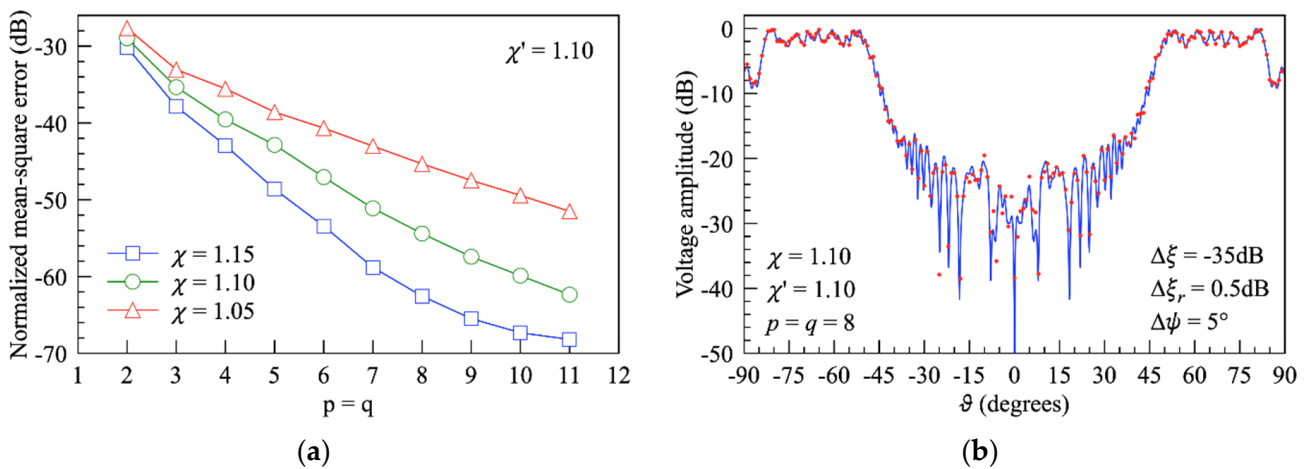


**Figure 10.** Relevant to the reconstruction of  $V_r$ : (a) Normalised mean-square errors; (b) Amplitude on the meridian at  $\varphi = 90^\circ$ . Blue solid line: exact. Red dots: recovered from the error-affected NF samples.

The overall effectiveness is confirmed by the FF reconstruction. The ones reported here refer to cut planes at  $\varphi = 90^\circ$  and  $\vartheta = 90^\circ$ . As can be seen, very good agreements also occur in this case. Note that the FF reconstruction at  $\vartheta = 90^\circ$  (see Figure 11b) is particularly significant, since this result can never be obtained using Hansen’s NF/FF transformation [15] modified to account for the presence of an infinite PEC ground plane without impairing the reconstruction with a severe truncation error.

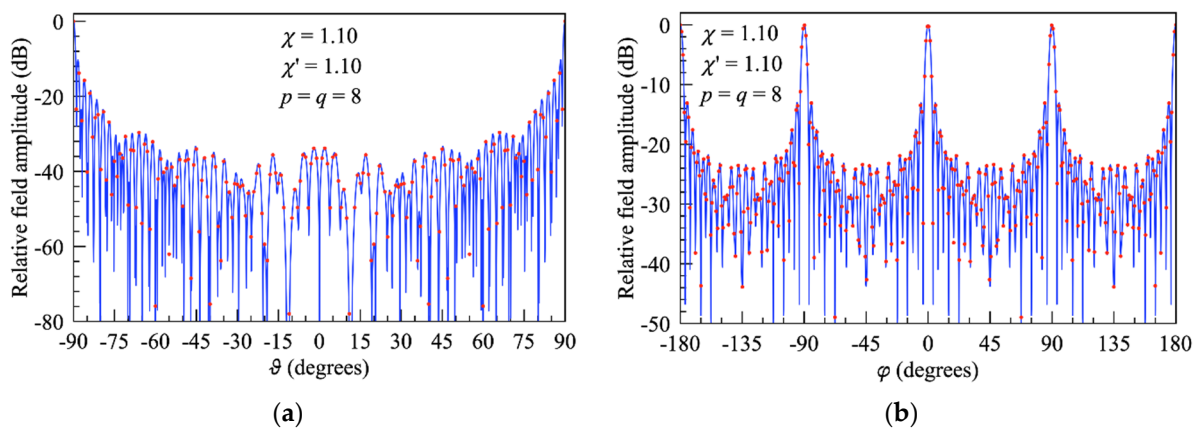


**Figure 11.** Far-field pattern. Blue solid line: exact. Red dots: interpolated from the non-redundant samples: (a)  $\vartheta$ —component on the cut plane at  $\varphi = 90^\circ$ ; (b)  $\vartheta$ —component on the cut plane at  $\vartheta = 90^\circ$ .

It is interesting to compare the number of NF samples collected over the upper hemisphere with that required by Hansen’s NF/FF transformation [15] in the presence of an infinite PEC ground plane. This last number is about one-half of that which would be required when the probe can be driven along the whole scan sphere. These comparisons are shown in Table 1 for both reported examples.

**Table 1.** Comparisons of the amount of required NF data.

AUT Case	Here Proposed	NF/FF Transformation [15] in Presence of PEC Ground Plane
Case A	14,521	20,736
Case B	13,297	36,864

As can be noted, in both the cases, the numbers of NF samples required by the devised sampling strategy are smaller than those needed by Hansen’s NF/FF transformation [15] in the presence of an infinite PEC ground plane, and this reduction reflects in a significant reduction in measurement time. Note that the devised approach also offers the possibility of recovering the NF data of the classical spherical lattice lying on the equator, otherwise zeroed when executing Hansen’s NF/FF transformation [15].

#### 4. Conclusions

In this paper, a non-redundant NF/FF transformation with a hemispherical scan for volumetric AUTs having one or two predominant dimensions as compared to the other one(s) has been developed. It makes use of the image principle to properly take into account the presence of the PEC ground plane, ensuring the repeatability of the measurements when dealing with heavy antennas. Moreover, it adopts a very flexible source model to reduce the volumetric redundancy of the combined AUT (AUT plus its image), which results when tackling the problem in its equivalent formulation, according to the image principle. This modelling is able to fit any kind of volumetric AUT, since a proper choice of its parameter allows one to develop a sampling representation using the minimum number of NF samples. A mirroring rule is used to synthesise the NF data, which would be collected if the scanning were carried out over the whole sphere and not just on the upper hemisphere. Then, the acquired and synthesised NF samples have been effectively interpolated via an efficient OSI algorithm to evaluate the NF value at any point of the classical grid required by Hansen’s NF/FF transformation [15]. It is so possible to avoid that a severe truncation error affects the FF reconstruction, as occurs if the NF data required by the NF/FF transformation [15] and falling on the lower hemisphere were not available.

The numerical results have assessed the reliability and precision of the devised sampling strategy and of the corresponding OSI algorithm.

**Author Contributions:** Conceptualization, F.F., C.G. and R.G.; Methodology, F.F. and R.G.; Software, F.F.; Validation, F.F.; Formal analysis, F.F., R.G. and G.R.; Investigation, F.F.; Writing—original draft, R.G.; Writing—review & editing, C.G., R.G. and G.R.; Visualization, G.R.; Supervision, C.G. All authors have read and agreed to the published version of the manuscript.

**Funding:** This research received no external funding.

**Data Availability Statement:** Data is contained within the article.

**Conflicts of Interest:** The authors declare no conflict of interest.

## References

1. Yaghjian, A.D. An overview of near-field antenna measurements. *IEEE Trans. Antennas Propag.* **1986**, *34*, 30–45. [[CrossRef](#)]
2. Appel-Hansen, J.; Dyson, J.D.; Gillespie, E.S.; Hickman, T.G. Antenna measurements. In *The Handbook of Antenna Design*; Rudge, A.W., Milne, K., Olver, A.D., Knight, P., Eds.; Peter Peregrinus: London, UK, 1986; pp. 584–694.
3. Gillespie, E.S. (Ed.) Special Issue on near-field scanning techniques. *IEEE Trans. Antennas Propag.* **1988**, *36*, 727–901.
4. Francis, M.H.; Wittmann, R.W. Near-field scanning measurements: Theory and practice. In *Modern Antenna Handbook*; Balanis, C.A., Ed.; John Wiley & Sons Inc.: Hoboken, NJ, USA, 2008; pp. 929–976.
5. *IEEE Standard 1720-2012*; IEEE Recommended Practice for Near-Field Antenna Measurements. Francis, M.H. (Ed.) IEEE: Piscataway, NJ, USA, 2012.
6. Sierra Castañer, M.; Foged, L.J. *Post-Processing Techniques in Antenna Measurement*; SciTech Publishing IET: London, UK, 2019.
7. Parini, C.; Gregson, S.; McCormick, J.; Van Rensburg, D.J. *Theory and Practice of Modern Antenna Range Measurements*; SciTech Publishing IET: London, UK, 2020.
8. Gennarelli, C.; Ferrara, F.; Guerriero, G.; D’Agostino, F. *Non-Redundant Near-Field to Far-Field Transformation Techniques*; SciTech Publishing IET: London, UK, 2022.
9. Jensen, F. On the probe compensation for near-field measurements on a sphere. *Archiv Elektr. Übertr.* **1975**, *29*, 306–308.
10. *NBSIR 75-809*; Non-Planar Near-Field Measurements: Spherical Scanning. Wacker, P.F. (Ed.) National Institute of Standards and Technology: Boulder, CO, USA, 1975.
11. Larsen, F.H. Probe correction of spherical near-field measurements. *Electr. Lett.* **1977**, *13*, 393–395. [[CrossRef](#)]
12. Yaghjian, A.D. Simplified approach to probe-corrected spherical near-field scanning. *Electr. Lett.* **1984**, *20*, 195–196.
13. Yaghjian, A.D.; Wittmann, R.C. The receiving antenna as a linear differential operator: Application to spherical near-field measurements. *IEEE Trans. Antennas Propag.* **1985**, *33*, 1175–1185. [[CrossRef](#)]
14. Hansen, J.E.; Jensen, F. Spherical near-field scanning at the technical university of Denmark. *IEEE Trans. Antennas Propag.* **1988**, *36*, 734–739. [[CrossRef](#)]
15. Hald, J.; Hansen, J.E.; Jensen, F.; Larsen, F.H. *Spherical Near-Field Antenna Measurements*; Hansen, J.E., Ed.; Peregrinus: London, UK, 1998.
16. Bucci, O.M.; Gennarelli, C.; Riccio, G.; Savarese, C. Data reduction in the NF-FF transformation technique with spherical scanning. *J. Electromagn. Waves Appl.* **2001**, *15*, 755–775. [[CrossRef](#)]
17. Laitinen, T.; Pivnenko, S.; Breinbjerg, O. Application of the iterative probe correction technique for a high-order probe in spherical near-field antenna measurements. *IEEE Antennas Propag. Mag.* **2006**, *48*, 179–185. [[CrossRef](#)]
18. Laitinen, T.; Pivnenko, S. Probe correction technique for symmetric odd-order probes for spherical near-field antenna measurements. *IEEE Antennas Wirel. Propag. Lett.* **2007**, *6*, 635–638. [[CrossRef](#)]
19. Laitinen, T.; Breinbjerg, O. A first/third-order probe correction technique for spherical near-field antenna measurements using three probe orientations. *IEEE Trans. Antennas Propag.* **2008**, *56*, 1259–1268. [[CrossRef](#)]
20. Laitinen, T. Double  $\varphi$ -step  $\theta$ -scanning technique for spherical near-field antenna measurements. *IEEE Trans. Antennas Propag.* **2008**, *56*, 1633–1639. [[CrossRef](#)]
21. Laitinen, T. Modified  $\theta$ -scanning technique for first/third-order probes for spherical near-field antenna measurements. *IEEE Trans. Antennas Propag.* **2008**, *57*, 1590–1596. [[CrossRef](#)]
22. Laitinen, T.; Pivnenko, S.; Nielsen, J.M.; Breinbjerg, O. Theory and practice of the FFT/matrix inversion technique for probe-corrected spherical near-field antenna measurements with high-order probes. *IEEE Trans. Antennas Propag.* **2010**, *58*, 2623–2631. [[CrossRef](#)]
23. Hansen, T.B. Spherical near-field scanning with higher-order probes. *IEEE Trans. Antennas Propag.* **2011**, *59*, 4049–4059.
24. Cornelius, R.; Heberling, D. Spherical wave expansion with arbitrary origin for near-field antenna measurements. *IEEE Trans. Antennas Propag.* **2017**, *65*, 4385–4388. [[CrossRef](#)]
25. Cornelius, R.; Heberling, D. Spherical near-field scanning with pointwise probe correction. *IEEE Trans. Antennas Propag.* **2017**, *65*, 995–996. [[CrossRef](#)]

26. D'Agostino, F.; Ferrara, F.; Gennarelli, C.; Guerriero, R.; Migliozi, M. Effective antenna modellings for NF-FF transformations with spherical scanning using the minimum number of data. *Int. J. Antennas Propag.* **2011**, *2011*, 936781. [[CrossRef](#)]
27. D'Agostino, F.; Ferrara, F.; Gennarelli, C.; Guerriero, R.; Migliozi, M. Non-redundant spherical NF—FF transformations using ellipsoidal antenna modeling: Experimental assessments. *IEEE Antennas Propag. Mag.* **2013**, *55*, 166–175. [[CrossRef](#)]
28. D'Agostino, F.; Ferrara, F.; Gennarelli, C.; Guerriero, R.; Migliozi, M. A spherical near-to-far-field transformation using a non-redundant voltage representation optimized for non-centered mounted quasi-planar antennas. *Electronics* **2020**, *9*, 944. [[CrossRef](#)]
29. Varela, F.R.; Iragüen, B.G.; Sierra Castañer, M. Fast spherical near-field to far-field transformation for offset-mounted antenna measurements. *IEEE Antennas Wirel. Propag. Lett.* **2020**, *19*, 2255–2259. [[CrossRef](#)]
30. Hansen, T.B. Numerical investigation of the system-matrix method for higher-order probe correction in spherical near-field antenna measurements. *Int. J. Antennas Propag.* **2012**, *2012*, 493705. [[CrossRef](#)]
31. Qureshi, M.A.; Schmidt, C.H.; Eibert, T.F. Adaptive sampling in spherical and cylindrical near-field antenna measurements'. *IEEE Antennas Propag. Mag.* **2013**, *55*, 243–249. [[CrossRef](#)]
32. Saccardi, F.; Rossi, F.; Mioc, F.; Foged, L.J.; Iversen, P.O. Application of the translated-SWE algorithm for the characterization of antennas installed on cars using a minimum number of samples. In Proceedings of the Antenna Measurement Techniques Association Symposium, Atlanta, GE, USA, 15–20 October 2017; pp. 1–6.
33. Bucci, O.M.; Gennarelli, C.; Savarese, C. Representation of electromagnetic fields over arbitrary surfaces by a finite and nonredundant number of samples. *IEEE Trans. Antennas Propag.* **1998**, *46*, 351–359.
34. D'Agostino, F.; Ferrara, F.; Gennarelli, C.; Guerriero, R.; Riccio, G. Pattern reconstruction of 3-D modular antennas by means of a non-redundant near-field spherical scan. *Electronics* **2022**, *11*, 2060. [[CrossRef](#)]
35. Camacho-Perez, J.R.; Moreno, P. Initial considerations towards hemispherical near-field antenna measurements. *IEEE Antennas Wirel. Propag. Lett.* **2014**, *13*, 1441–1444. [[CrossRef](#)]
36. Mauermayer, R.A.M.; Eibert, T.F. Spherical field transformation above perfectly electrically conducting ground planes. *IEEE Trans. Antennas Prop.* **2018**, *66*, 1465–1478.
37. Harrington, R.F. *Time-Harmonic Electromagnetic Fields*; John Wiley & Sons, Inc.: New York, NY, USA, 2001.
38. D'Agostino, F.; Ferrara, F.; Gennarelli, C.; Guerriero, R.; Migliozi, M. A non-redundant spherical NF/FF transformation for an AUT measured over an infinite perfectly conducting ground plane. In Proceedings of the Antennas Propagation Conference, Birmingham, UK, 11–12 November 2019; pp. 1–5.
39. D'Agostino, F.; Ferrara, F.; Gennarelli, C.; Guerriero, R.; Migliozi, M. AUT far-field pattern reconstruction from a reduced set of spherical near-field data collected in presence of an infinite perfectly conducting ground plane. In Proceedings of the European Conference on Antennas and Propagation, Copenhagen, Denmark, 15–20 March 2020; pp. 1–5.
40. Bucci, O.M.; D'Elia, G.; Migliore, M.D. Advanced field interpolation from plane-polar samples: Experimental verification. *IEEE Trans. Antennas Propag.* **1998**, *46*, 204–210. [[CrossRef](#)]

**Disclaimer/Publisher's Note:** The statements, opinions and data contained in all publications are solely those of the individual author(s) and contributor(s) and not of MDPI and/or the editor(s). MDPI and/or the editor(s) disclaim responsibility for any injury to people or property resulting from any ideas, methods, instructions or products referred to in the content.